

Study of hard and electromagnetic processes at CERN-SPS energies: an investigation of the high- μ_B region of the QCD phase diagram with NA60+

NA60+ Collaboration*

Abstract

The exploration of the phase diagram of Quantum ChromoDynamics (QCD) is carried out by studying ultrarelativistic heavy-ion collisions. The energy range covered by the CERN SPS ($\sqrt{s_{NN}} \sim 6\text{--}17$ GeV) is ideal for the investigation of the region of the phase diagram corresponding to finite baryochemical potential (μ_B), and has been little explored up to now. We propose in this document a new experiment, NA60+, that would address several observables which are fundamental for the understanding of the phase transition from hadronic matter towards a Quark–Gluon Plasma (QGP) at SPS energies. In particular, we propose to study, as a function of the collision energy, the production of thermal dimuons from the created system, from which one would obtain a caloric curve of the QCD phase diagram that is sensitive to the order of the phase transition. In addition, the measurement of a ρ – a_1 mixing contribution would provide conclusive insights into the restoration of the chiral symmetry of QCD. In parallel, studies of heavy quark and quarkonium production would also be carried out, addressing the measurement of transport properties of the QGP and the investigation of the onset of the deconfinement transition. The document also defines an experimental set-up which couples a vertex telescope based on monolithic active pixel sensors (MAPS) to a muon spectrometer with tracking (GEM) and triggering (RPC) detectors within a large acceptance toroidal magnet. Results of physics performance studies for most observables accessible to NA60+ are discussed, showing that the results of the experiment would lead to a significant advance of our understanding of strong interaction physics. The document has been submitted as an input to the European Particle Physics Strategy Update 2018–2020 (<http://europeanstrategyupdate.web.cern.ch/>).

December 20, 2018

*See Appendix for the list of collaboration members

1 Introduction and QCD phase diagram

Quantum ChromoDynamics (QCD), the theory of the strong force, has a rich phase structure. On the one hand, asymptotic freedom allows it to completely define the degrees of freedom in terms of quarks and gluons, while on the other hand hadrons become the relevant degrees of freedom when confinement sets in. For a system in thermodynamic equilibrium, temperature (T) and baryochemical potential (μ_B) are intensive parameters that are the same for any of its subsystems. It is convenient to describe the phase diagram, as shown in the left panel of Fig. 1, in terms of these intensive parameters both from the perspective of lattice QCD in which the two are used as independent variables, and in the application of a grand-canonical ensemble in the analyses of heavy-ion experiments. Our quantitative understanding of the QCD phase diagram is largely restricted to the region of low μ_B . For $\mu_B \sim 0$, lattice QCD provides quantitative results (see Fig. 1-right): a fast increase of ε/T^4 (ε = energy density) occurs around a critical temperature $T_c \approx 155$ MeV. In this regime, the phase transition is a cross-over [1, 2].

The extensive experimental campaigns conducted at the CERN-SPS, BNL-RHIC and CERN-LHC accelerators have mostly explored so far this region of the phase diagram at low μ_B , showing that a deconfined state of matter is produced in heavy-ion collisions at high energies, with properties consistent with the predictions of lattice QCD. Present experiments at RHIC and SPS started in recent years to address features of the phase diagram structure at large μ_B . For moderate temperatures and high baryon densities the existence of a first order phase transition with co-existence of a mixed-phase was suggested. The first order transition line should end with a second order critical point. The existence of such a critical point and a first-order phase transition remain to be confirmed in experiments. Evidence for a first order phase transition can be provided by the measurement of the caloric curve. A direct measurement of such a curve for the phase transition between a hadron gas and a QGP can be based on precise temperature measurements as a function of the centre of mass energy.

Chiral symmetry is spontaneously broken in the hadronic world due to the formation of quark and gluon condensates. This leads to the generation of the hadron mass splittings in the light hadron spectrum of ~ 0.5 GeV for the chiral partners π - σ and ρ - a_1 . Lattice QCD calculations for $\mu_B = 0$ show that at the hadron-QGP phase transition boundary the chiral condensate steeply decreases around T_c , indicating the approach to chiral restoration [3].

Precise measurements of heavy quarkonium states can be used to study the suppression of such states due to colour screening which is considered a key signature of a deconfined state. On the other hand, open charm measurements allow us to extract fundamental transport coefficients from the QGP as well as improve our understanding of hadronization mechanisms.

We propose a new experiment, NA60+, as a follow-up experiment to NA60 [4, 5] to address each of these sets of observables through very high precision measurements in Pb-Pb collisions in the finite μ_B region of the phase diagram where such measurements either have not been done, or have not yet reached a level of precision that would allow for meaningful constraints on theoretical models. In the following section 2, we discuss the NA60+ physics plans and how they will address each of the aforementioned observables through high precision dimuon and hadronic measurements. In the sections 3 and 4 we detail the requirements to accomplish this programme in terms of collision energies, integrated luminosities that allow for meaningful measurements, and proposed detector technologies, respectively. Based on those requirements, section 5 provides projections for the physics performance for each of the observables discussed in section 2. This is followed by a brief overview of other initiatives in terms of present and future detectors/facilities in section 6 and our conclusions in strong favour of the NA60+ project in section 7.

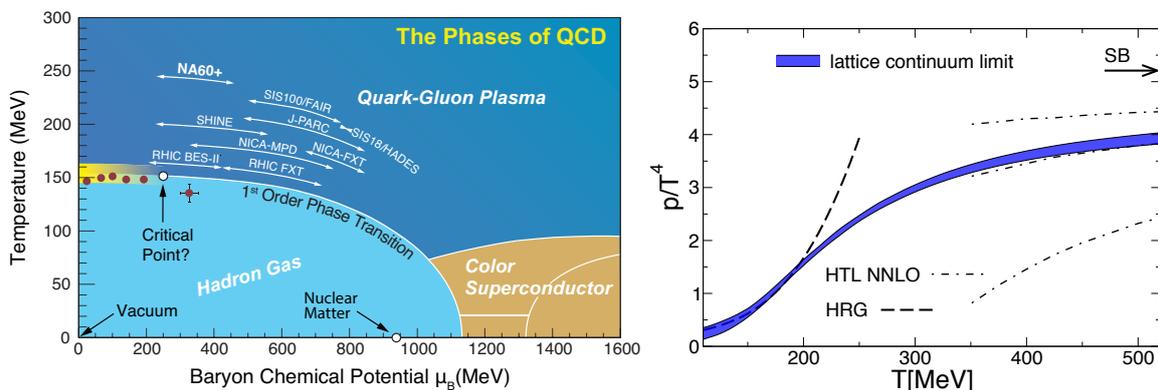


Fig. 1: The QCD phase diagram (left panel, courtesy of Thomas Ullrich) and the equation of state $P(T)/T^4$ in the limit of vanishing baryon density [1] measured on the lattice (right panel): the latter is characterized by a rise in the effective number of active degrees of freedom, indicating the cross-over transition to a QGP.

2 Observables/Measurements

2.1 Thermal radiation

2.1.1 Chiral symmetry restoration: measurement of ρ - a_1 chiral mixing

A long-standing question is how chiral symmetry restoration manifests itself in the hadron spectrum, i. e. what are its observable consequences. The NA60 experiment precisely measured the ρ spectral properties in In–In collisions at $\sqrt{s_{NN}} = 17.3$ GeV [5–7] to be in agreement with a microscopic many-body model predicting a very strong broadening with essentially no mass shift [8, 9]. To understand if the ρ melting is a signal of the restoration of chiral symmetry, and more in general to understand the changes in the hadron spectrum, a study of the spectral properties of its chiral partner a_1 is fundamental. We present here our proposal to investigate the ρ - a_1 chiral mixing towards chiral symmetry restoration.

There is no direct coupling of axial states to the dilepton channel, so that in vacuum the $e^+e^- \rightarrow$ hadrons cross section has a dip in the a_1 mass range [10]. However, in the medium, for dilepton masses above 1 GeV, 4 pion (and higher) states dominate the free electromagnetic correlator. Model-independent predictions of chiral symmetry show that to leading order in temperature one has a pion-induced mixing of vector (V) and axial-vector (A) correlators [11]: $\Pi_V(T) = (1 - \varepsilon)\Pi_V^{vac} + \varepsilon\Pi_A^{vac}$ where ε is the mixing parameter ($\varepsilon = T^2/6f_\pi^2$, $f_\pi = 93$ MeV, and $\varepsilon \sim 0.5$ at chiral symmetry restoration). The admixture of the a_1 resonance, via the axial-vector correlator, thus entails an enhancement of the dilepton rate for $M \sim 1$ –1.4 GeV. A precision measurement of this enhancement for $M > 1$ GeV sheds light on the ρ - a_1 chiral mixing and the approach to chiral symmetry restoration.

To optimize the dilepton signal of interest, the lifetime of matter around T_c should be maximized relative to other contributions: starting out in a (soft) mixed phase is a key point to enhance the effects related to chiral restoration. Thus the collision energy should be large enough to produce this matter, but small enough not to overshoot it producing partonic matter. This is expected to occur at collision energies somewhat smaller than $\sqrt{s_{NN}} = 17$ GeV, close to the onset of deconfinement, where the QGP yield is negligible. The optimal energy range of interest can be then established by the medium temperature measurement, as detailed in section 2.1.2.

A calculation of the dilepton thermal yield with no chiral mixing and full chiral mixing at $\sqrt{s_{NN}} = 8.8$ GeV ($\varepsilon = 1/2$) has been performed within the framework of [12]. The chiral mixing will fill the dip in the mass range 1–1.4 GeV with a yield increase of $\sim 30\%$.

2.1.2 Hadron–QGP phase transition: measurement of the strongly interacting matter caloric curve at high μ_B

The measurement of a caloric curve provided evidence for a first order phase transition from the liquid self-bound nuclear ground state to a gas of free nucleons [13]. We present here the method to perform the first measurement of a caloric curve for the phase transition between the hadron gas and the QGP. The temperature measurement, performed as a function of collision energy, is based on a precise *dimuon* thermometer.

For dilepton masses above 1.5 GeV, the continuum of overlapping resonances leads to a flattened spectral density corresponding to a simpler description in terms of quarks and gluons (hadron-parton duality). Here medium effects on the electromagnetic spectral function (Π_{EM}) are parametrically small, of the order of $(T/M)^2$, providing a stable thermometer. With $\Pi_{EM} \propto M^2$, and in non-relativistic approximation, one has $dN/dM \propto M^{3/2} \exp(-M/T_s)$ [12]. Since mass is by construction a Lorentz-invariant, the mass spectrum is immune to any motion of the emitting sources, unlike transverse momentum (p_T) spectra. The parameter T_s in the spectral shape of the mass spectrum is therefore a space-time average of the thermal temperature T over the fireball evolution. The choice of the mass window, 1.5–2.5 GeV, implies $T \ll M$ and thus strongly enhances the sensitivity to the early high- T phases of the evolution. This method has been exploited by NA60 to measure the medium temperature in In–In collisions at $\sqrt{s_{NN}} = 17.3$ GeV. The fit of the mass spectrum gives $T_s = 205 \pm 12$ MeV [5, 7]. This is above T_c , thus showing that the QGP is produced at this collision energy.

The evolution of the initial temperature and T_s vs collision energy has been studied theoretically in [12] in the interval $\sqrt{s_{NN}} = 6$ –200 GeV. However, in this calculation a cross-over transition is assumed. The average temperature T_s from the mass fit is about 30% below the corresponding initial one at $\sqrt{s_{NN}} = 200$ GeV. The two temperatures are both close to the critical temperature below $\sqrt{s_{NN}} = 10$ GeV, with their gap reducing to less than 15%. This is largely due to the (pseudo-)latent heat in the transition which needs to be burned off in the expansion/cooling. The collision energy range below $\sqrt{s_{NN}} = 10$ GeV thus appears to be essential to map out the phase-transition regime at high μ_B , with the possible discovery of a plateau in the caloric curve built with dilepton slopes T_s . The experimental programme of NA60+ thus proposes to perform an energy scan in the interval $\sqrt{s_{NN}} = 6$ –17 GeV ($E_{lab} = 20$ –160 GeV/nucleon).

2.1.3 Thermal dilepton excitation function and fireball lifetime

A precise measurement of the thermal dilepton excitation function—the total yield of low mass thermal dileptons—is also sensitive to the fireball lifetime. It was shown in [12] that the integrated thermal excess radiation in $0.3 < M < 0.7$ GeV tracks the total fireball lifetime remarkably well, within less than 10%. The NA60 measurement in In–In at $\sqrt{s_{NN}} = 17.3$ GeV allowed the fireball lifetime to be constrained with unprecedented precision: $\tau_{fb} = 7 \pm 1$ fm/c [12]. Thus, low-mass dileptons are an excellent tool to detect *anomalous* variations in the fireball lifetime due, for instance, to the presence of a soft mixed phase: an increase in τ_{fb} with identical final-state hadron transverse momentum spectra (i. e. in terms of radial-flow) would necessarily imply a lifetime extension without extra collective flow, i. e. a soft phase.

2.2 Quarkonium

A suppression of heavy quarkonium states due to a colour screening mechanism has been considered, from the very beginning of this field, as one of the key signatures for the formation of a deconfined state [14]. Detailed studies, in particular for the J/ψ meson, were first performed at top SPS energy (centre of mass energy per nucleon–nucleon collision $\sqrt{s_{NN}} = 17.3$ GeV) [15]. More recently, extensive sets of measurements were obtained, for both charmonium and bottomonium states, at the RHIC ($\sqrt{s_{NN}}$ up to 200 GeV) and LHC ($\sqrt{s_{NN}}$ up to 5.02 TeV) ion colliders [16, 17]. Concerning J/ψ , a $\sim 30\%$ suppression of the J/ψ production that could not be ascribed to cold nuclear matter effects alone was observed in central Pb–Pb collisions at the SPS by the NA50/NA60 experiments. The size of such an “anomalous” suppression is qualitatively consistent with the melting in the QGP of the χ_c and $\psi(2S)$ charmonium states, which would lead to a suppression of the J/ψ coming from the decay of those particles.

As of today, heavy quarkonium production in nucleus–nucleus collisions has not been studied below top SPS energy. NA60+ proposes to carry out a measurement of J/ψ production down to a decreased energy of the incident heavy-ion beam of approximately $E_{lab} = 40$ GeV/nucleon ($\sqrt{s_{NN}} = 8.8$ GeV). The possible effects of the formation of a QGP with increasing μ_B on charmonium states have not been thoroughly investigated by theory. On the one hand, the initial energy density of the system should decrease when moving to lower collision energies. Consequently, if the J/ψ suppression effects observed at top SPS energy are due to the dissociation of the χ_c and $\psi(2S)$ states, one should be able to detect the beam energy threshold for the onset of their suppression. By correlating this information with the corresponding measurement of the temperature via thermal dimuons, one could experimentally identify the threshold temperature for the melting of those charmonium states. In this way a crucial test of the corresponding lattice QCD predictions can be carried out. On the other hand, the formation of a baryon-rich QGP may have unexpected, and up to now never investigated, effects even on directly produced J/ψ , making this measurement even more appealing.

By moving to lower collision energies, there are also strong indications for an increase of the size of cold nuclear matter effects on the produced $c\bar{c}$ pair. Indeed, by studying J/ψ production in proton–nucleus collisions at 158 and 400 GeV incident energy [18], the NA60 experiment discovered a much stronger break-up effect on the final state J/ψ at the lower of the two energies. NA60+ proposes to extend such measurements to even lower energies, with a twofold interest. First, break-up effects in cold nuclear matter are not related to QGP formation, therefore they must be corrected for when evaluating any “anomalous” suppression in nucleus–nucleus collisions. Therefore, such data would be mandatory for a correct interpretation of nucleus–nucleus results. Second, the production and propagation of a bound $c\bar{c}$ state in cold nuclear matter is expected to be sensitive to various QCD-related phenomena, which include both initial state (nuclear shadowing) and final state effects (propagation of a colour singlet/octet pre-resonant state or the final resonance in the nucleus). Past fixed target experiments at various facilities (SPS, Tevatron, HERA) collected several sets of data, but the observations still lack a comprehensive interpretation, and new data at lower collision energy would access up to now unexplored specific kinematic configurations.

2.3 Open charm

Heavy-flavour measurements are providing unprecedented insights into the physics of hot QCD matter at small baryochemical potential, as produced at the heavy-ion colliders RHIC and LHC. With a focus on the low and intermediate momentum region, measurements of p_T distributions, compared to pp collisions, and of azimuthal anisotropies of D mesons are used for example to extract fundamental transport coefficients of the QGP, such as the heavy-quark diffusion coefficient (see e. g. Ref. [19]). Measurements of the strange-charm D_s^+ meson and of the Λ_c baryon, in comparison with D^0 and D^+ mesons containing only charm and light quarks, are used to characterize the hadronization mechanisms of charm quarks and the role of quark recombination [20].

It is of high interest to extend these studies into the region of finite chemical potential through heavy-ion collisions at lower energies. The charm diffusion coefficient is predicted to be larger in the hadronic phase at temperatures approaching the critical temperature $T_c \approx 150$ MeV from below than in the QGP phase at temperatures larger than T_c [21, 22]. It should then be possible to investigate this feature in Pb–Pb collisions at SPS energies, where the hadronic phase $T < T_c$ represents a large part of the space-time evolution of the collisions. Measurement of p_T distributions and azimuthal anisotropy should exhibit features induced by a strong collective behaviour. In addition, such measurements that are sensitive to interactions of charm in the hadronic phase would be important input also for precision estimates of diffusion coefficients at collider energies, where a rather extensive hadronic evolution from T_c down to the kinetic freeze-out temperature of $T \sim 100$ MeV occurs. For what concerns hadronization mechanisms, recombination effects could lead to a large enhancement of the Λ_c/D ratio. The enhancement could be larger at SPS than at RHIC and LHC energies, because of the larger baryon content of the fireball (the baryon number of the colliding nuclei is “stopped” in the collision region).

The total production cross section of $c\bar{c}$ pairs in hadronic collisions at centre-of-mass energies below 20 GeV has never been measured with high precision, because the yields at these energies are very small. The only measurements in nucleus–nucleus collisions at the SPS were obtained by the NA60 experiment in In–In collisions (using intermediate mass dimuons, with an uncertainty of about 20%) [5] and by the NA49 experiment in Pb–Pb collisions (upper limit using reconstructed D^0 decays) [23]. A precise measurement of this cross section in p–Pb and Pb–Pb collisions at the SPS, besides providing the optimal normalization for J/ψ production, is also predicted to be directly sensitive to chiral symmetry restoration. The melting of the $\langle\bar{q}q\rangle$ condensate might also shift the threshold for $D\bar{D}$ production from $2m_{D^0} \approx 3.73$ GeV in vacuum to about 3 GeV in the chirally-symmetric medium. This reduction is predicted to lead to an enhancement of

open charm meson yields by a factor of up to 7, with respect to binary scaling of the production in pA collisions. Thus, a large enhancement of D meson production is regarded as a signature for a chirally-symmetric phase [24].

Finally, measurements of D-meson production in proton–nucleus collisions at SPS energy can provide constraints to parameterisations of the nuclear modification of parton distribution functions (PDFs) at $Q^2 \sim 10\text{--}40 \text{ GeV}^2$ and large Bjorken- x of $x_{\text{Bj}} \sim 0.1\text{--}0.3$, depending on $p_{\text{T},c} \sim 0\text{--}3 \text{ GeV}/c$. In this kinematic region, which is poorly-constrained by existing data, the PDFs in large nuclei are expected to change from enhancement (anti-shadowing) at $x_{\text{Bj}} \sim 0.1$ to suppression (“EMC effect”) at $x_{\text{Bj}} \sim 0.3$ (see e. g. Ref. [25]). NA60+ could provide precise input via ratios of the D-meson production cross section in p–Pb or p–U collisions (maximal nuclear effects) and p–Be collisions (minimal nuclear effects).

3 Requirements (statistics, beams, installation)

The experimental programme requires to collect data at different energies (beam energy scan, BES) in the interval $\sqrt{s_{\text{NN}}} \sim 5\text{--}17 \text{ GeV}$. In order to reach the required precision for the proposed measurements, the statistics goal at each energy of BES is:

- $\geq 5 \cdot 10^7$ reconstructed thermal muon pairs (factor 100 increase over NA60 and $\sim 10^5$ over RHIC/LHC experiments);
- $\geq 3 \cdot 10^4$ reconstructed J/ψ ;
- $\geq 10^7$ reconstructed D^0 .

The proposed physics programme of NA60+ is based on high-intensity lead beams delivered by the CERN SPS. This facility is continuously running since many years. Thanks to the new injection scheme it would be able to deliver ion beams over the required energy interval with intensities exceeding 10^7 ions/s (in 5 s bursts, 15 s inter-bursts). An ion beam could be delivered to a fixed target experiment while the SPS is used as ion injector for LHC. Considering the present LHC running conditions with ions, this means that ions would be available for ~ 4 weeks per year. Tentatively, data should be collected at $E_{\text{lab}} = 20, 30, 40, 80, 120$ and 160 GeV/nucleon . Further energy points might be required depending on the findings. Corresponding periods of proton beams at a few energy points will be required for reference measurements (like open charm and Drell-Yan), with intensities of $\sim 5 \cdot 10^8$ protons/s.

The beam intensity dictates that the experiment must be installed underground. The only existing hall is the ECN3 in the CERN north area. This is presently under discussion within CERN Physics Beyond Colliders for running after LS3 during LHC Run 4 and Run 5.

4 The NA60+ experiment, layout and detectors

A sketch of the NA60+ apparatus is shown in Fig. 2. Muons are measured by a magnetic spectrometer placed after a hadron absorber. A magnet, which creates a toroidal field in the plane perpendicular to the beam direction, is placed in between the muon tracking stations and provides a field integral of 0.75 Tm at $R = 1 \text{ m}$. While the absorber provides the muon identification, it also degrades the kinematics of the muons, because of energy loss fluctuations and multiple scattering. This problem is overcome by measuring particle tracks also before the hadron absorber with a silicon tracker, which is the key element for a precision measurement of muons. Muon tracks are then matched to the tracks measured in the silicon vertex telescope (VT) in coordinate and momentum space. In addition, the VT provides also the measurement of the charged-particle multiplicity density, and hadronic decays of open charm. The apparatus covers the forward rapidity hemisphere, measuring muons in the pseudo-rapidity interval $1.6 < \eta < 4.5$. Moreover, the apparatus is designed to guarantee a good coverage down to low transverse momenta in particular for dimuons with low mass and low pseudo-rapidity. The set-up will be adapted to the varying beam energy by scaling the absorbers thickness and moving the position of the tracking stations in such a way to keep always a good acceptance close to mid-rapidity.

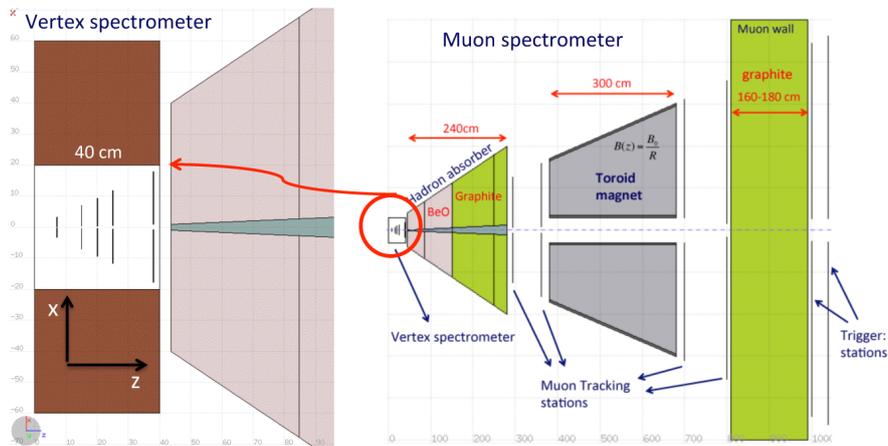


Fig. 2: Geometry of the proposed experimental apparatus.

We foresee two dedicated programmes, one with a proton beam on various nuclear targets (pA), and one with lead

beams on lead targets (Pb–Pb). For the Pb–Pb running, a segmented Pb target system of 10–15% interaction probability (4 mm thickness) will be used, whereas for pA collisions, different nuclear targets (Be, Al, Cu, In, W, Pb and U) with 1 mm thickness will be exposed simultaneously to the proton beam. The targets will be housed inside a vacuum box.

In the following subsections we briefly present the detector concept for the different sub-systems. Detailed performance features and simulations of the full detector response will be documented in a future Letter of Intent and Technical Design Reports at a later point.

4.1 Detector technology

4.1.1 Vertex telescope: pixel detector

The vertex telescope is a spectrometer consisting of 5 silicon pixel tracking planes immersed in a 1.2 Tm dipole field (see Fig. 2). The tracker will be based on CMOS Monolithic Active Pixel Sensors (MAPS), which are now reaching impressive performances, almost ideal in many respects. At present, the state of the art is the pixel sensor ALPIDE developed for the new ALICE inner tracker. Based on the 0.18 μm CMOS imaging commercial technology by TowerJazz, this $15 \times 30 \text{ mm}^2$ sensor features a pixel size of $27 \times 29 \mu\text{m}^2$ with a thickness of just 50 μm [26]. At $\sim 1 \text{ MHz}$ Pb–Pb interaction rate, the hit flux reaches $\sim 50 \text{ MHz/cm}^2$ in the tracking station closest to the interaction point. The ALPIDE sensor can be operated up to $\sim 100 \text{ MHz/cm}^2$ but the readout rate is limited to $\sim 10 \text{ MHz/cm}^2$.

For NA60+ we will pursue, in close synergy with the ALICE experiment, a new generation of MAPS with almost ideal characteristics: very large area up to $\sim 14 \times 14 \text{ cm}^2$, retaining thickness of 50 μm or less. The key idea is to use stitching, a technology that allows an image sensor that is larger than the field of view of the lithographic equipment to be fabricated. In this way, sensors of arbitrary size can be manufactured, the only limit being the size of the wafers. The basic unit might be a sensor of size $1.5 \times 14 \text{ cm}^2$ [27]. A resulting wafer-scale sensor could be obtained at this stage replicating this sensor chip several times along the periphery side. Such a matrix amounts to 5000×5000 pixels. The sensor is meant to be operated in continuous mode, recording frames at $\sim 5\text{--}10 \text{ MHz}$ rate. The amount of memory buffers and serial data transmitters, all placed in the periphery, will be determined to match the required readout band-width.

All tracking stations will be identical, consisting of just few large sensors leading to a modular, more robust and cheaper layout that allows simple replacement of non working sensors. A tracking station with few large sensors where power distribution is totally managed internally will mainly eliminate the need of a mechanical and electrical support, confining the interconnection to the outside world to the sensor edges, including the cooling. With a flex circuit for power distribution the material budget for such tracking stations might drop to a breakthrough level of 0.1% X_0 .

4.1.2 Muon tracking: GEMs

Gas Electron Multiplier (GEM) foils [28] are structures commonly used as proportional counters, due to their excellent performance at high particle rates. Being successfully employed in many experiments, such as COMPASS [29], LHCb [30] or TOTEM [31], GEMs have become the solution for the upcoming upgrades of the CMS Muon Endcap [32] or the ALICE TPC [33].

GEM detectors use copper-clad polyimide foil with etched holes for gas amplification. Thanks to the photo-lithography methods used in the production process of GEM foils, the size of the amplification region could be reduced to a sub-millimetre level (typical hole diameter of 50–70 μm with a pitch of 140 μm). This allows GEMs to be operated at high particle rates of 1 MHz/cm^2 [30] with a very good spatial resolution of $\mathcal{O}(100 \mu\text{m})$ or smaller [29]. A cascade of GEM foils permits one to attain very high proportional gains without the occurrence of discharges. Since the development and perfection of the single-mask technique [34], high-quality large-area GEMs can be produced allowing to cover substantial detector surfaces at relatively low costs. All that makes the GEM technology well suited for a high-rate muon tracker to be employed in the NA60+ spectrometer. Following the schematic layout presented at the beginning of this section the total active area of the muon tracker is $\sim 116 \text{ m}^2$, organized in 4 tracking stations, behind the hadron absorber. We foresee two modules per station to improve tracking capabilities of the system (position resolution, background rejection). A single tracking module (chamber) will employ a triple GEM amplification structure with a short drift gap of $\mathcal{O}(3 \text{ mm})$ and strip readout. Due to the raw-material related constraints on the maximum width of GEM foils (60 cm), we foresee a single chamber to be a $\sim 50 \times 100 \text{ cm}^2$ rectangle. Taking into account the active area of the tracker and the dimensions of a single chamber, a total number of ~ 1500 GEMs will have to be produced (including spares) in order to assemble more than 450 tracking modules. We propose to use cost-effective, non-flammable Ar-based gas mixtures with carbon dioxide (CO_2) as a quencher. In order to improve time resolution of the tracking module an addition of Tetrafluoromethane (CF_4) is considered. Both Ar/ CO_2 and Ar/ CO_2 / CF_4 mixtures have been successfully used in currently operated high-rate trackers (e. g. COMPASS or LHCb) without notable ageing effects.

Because of the large total area of the muon tracker, a pad readout would lead to an excessively large number of front-end electronics (FEE) channels. The latter can be reduced by employing 2D strip readout [29]. Given the chamber dimensions and assuming 200 μm spatial resolution, a strip pitch of $\mathcal{O}(1 \text{ mm})$ results in almost 900 thousand of FEE channels. Further improvement of the spatial resolution may be realized by employing a zigzag strip geometry [35] or utilizing pad readout in the innermost part of the tracker.

For the readout, we consider using a VFAT chip [36], successfully employed in TOTEM and ATLAS forward detectors and planned for the CMS GEM chambers, or the new VMM3 chip [37] developed for the ATLAS New Small Wheel upgrade. Detailed performance studies will be performed for the final assessment.

4.1.3 Muon triggering: RPCs

Resistive Plate Chambers (RPC) were used in LHC experiments for large surface tracking devices and may represent a viable choice for the muon triggering system of the NA60+ experiment. In particular, these detectors were adopted for the ALICE forward muon arm, which had a conceptual structure similar to the one proposed for NA60+. Following that set-up, one can envisage a system composed of two stations, each one featuring two RPC planes. This set-up would allow a trigger condition where one requires three out of four planes fired, providing the necessary redundancy in case of local inefficiencies in the detection planes. The single-gap detectors, with Bakelite electrodes, can be read on both sides with orthogonal strips with a pitch varying from 1 to 4 cm, following the expected occupancy and the needed spatial resolution. The detectors could be operated with a FEE which includes an amplification stage, in order to reduce the charge delivered inside the gas gap, improving both rate capability ($> 100 \text{ Hz/cm}^2$) and detector lifetime. An R&D programme is ongoing in order to replace the flammable gas mixture used, e. g. in ALICE with non-flammable and low-GWP gas.

A possible issue that needs investigation is related to the area of the detection planes, since, presently, the maximum size of Bakelite electrodes available is about $300 \times 180 \text{ cm}^2$. With a transverse size of the detector of $\sim 8 \text{ m}$, the simple arrangement adopted in ALICE (two detectors, symmetrically positioned with respect to the beam axis) will not be possible, and some integration studies will be needed in order to devise a practical solution which ensures sufficient overlaps and avoid dead zones.

4.1.4 Muon magnet

A magnet similar to the ACM [38] used by NA60 is needed with larger dimensions: length of $\sim 3 \text{ m}$, radius at entrance $0.3 < R < 1.65 \text{ m}$, radius at exit $R = 2.95 \text{ m}$, field $B \cdot R \sim 0.2\text{--}0.25 \text{ Tm}$. The ACM was an open toroid with field circling the beam-axis. The windings of the ACM were arranged in a complicated way, providing an excellent field quality but making this magnet difficult to build and expensive. We propose a “minimal” design, easier to build and cheaper, but with a more complex field [39]. This layout could also be useful for other experiments. The main part consist of a central cylinder of 0.6 m diameter and 3 m length in the beam direction, build up out of 8 sectors. The sectors are tangentially displaced with respect to the cylinder axis in order to cross the current from one segment to another. The dimensions of the radial conductors are chosen to give little obstruction for incoming particles. The outer connection of the radial conductors is not critical. A segment consists out of a single winding, the straight conductors joined by screws. The idea is to get an easy scalable, meccano-like structure. This simple concept of minimal amount of windings has to be tested on field homogeneity and acceptance. For reasons of simplicity and cost efficiency it is proposed to add segments if the field homogeneity needs to be increased, instead of adding more outer conductors to the radial ones. Since the total current remains the same, this will not affect the acceptance. In order to reduce energy consumption the magnet will be pulsed. To avoid overheating of the central conductor, coolant has to be flown through it. It can be made laminated or foreseen of tubes. If the field quality is not satisfying due to current inhomogeneity, one can try a laminated central conductor with loop for each lamination.

5 Physics performances

5.1 Thermal dileptons: caloric curve, ρ - a_1 chiral mixing, excitation function

Detailed performance studies were carried out for 5% most central Pb–Pb collisions at $\sqrt{s_{\text{NN}}} = 6.3, 8.8$ and 17.3 GeV . The differential spectra of thermal $\mu^+\mu^-$ pairs, $d^3N/(dMdp_T dy)$, are based on the in-medium ρ , ω and 4π spectral functions, QGP and the expanding thermal fireball model of [12]. The generator is based on the model calculation which assumes either no ρ - a_1 chiral mixing or full chiral mixing ($\varepsilon = 1/2$) in the mass region $1 < M < 1.5 \text{ GeV}$. For the performance of the temperature measurement, thermal dileptons were generated without chiral mixing. The hadron cocktail generator for the 2-body decays of η , ω , and ϕ and the Dalitz decays $\eta \rightarrow \gamma\mu^+\mu^-$ and $\omega \rightarrow \pi^0\mu^+\mu^-$ is based on the NA60 generator and on the statistical model of [40]. The Drell-Yan process and open-charm production are simulated with the PYTHIA event generator.

We present the results for a sample of $2 \cdot 10^7$ reconstructed pairs in central collisions at each energy, corresponding to a total sample of $\sim 5 \cdot 10^7$ integrated in centrality at each energy. The left panel of Fig. 3 shows the signal reconstructed mass spectra (black) for $\sqrt{s_{\text{NN}}} = 8.8 \text{ GeV}$ after subtraction of the combinatorial background due to pion and kaon decays as well as fake matches. The latter arise from incorrect matches of a muon track to a track reconstructed in the VT. The combinatorial background is subtracted assuming a 0.5% systematic uncertainty (shown as a yellow band). For what concerns minimum bias collisions, the progress in statistics over NA60 is a factor ~ 100 , retaining a similar background ratio and a better mass resolution. At a $\sim 1 \text{ MHz}$ interaction rate, this statistics can be collected in a ~ 30 days run. The figure shows all the expected signal components. For $M < 1 \text{ GeV}$, the thermal radiation yield is dominated by the in-medium ρ . The ω and ϕ peaks are well resolved with a resolution of $\sim 10 \text{ MeV}$ at the ω mass. The thermal spectrum is measurable up to $2.5\text{--}3 \text{ GeV}$. The open charm yield becomes totally negligible at low energy. The Drell-Yan yield will be measured in dedicated pA runs (see also section 5.3). The thermal spectra are obtained after (i) subtraction of the hadronic cocktail for $M < 1 \text{ GeV}$ of ϕ , ω and η decays into $\mu^+\mu^-$ and the ω , η Dalitz decays and (ii) subtraction of Drell-Yan and open charm muon pairs for $M > 1 \text{ GeV}$. After acceptance correction the spectra are fit with $dN/dM \propto M^{3/2} \exp(-M/T_s)$ in the interval $M = 1.5\text{--}2.5 \text{ GeV}$. This is shown in the right panel of Fig. 3.

The resulting temperatures are compared to the theoretical model used as an input in the left panel of Fig. 4. At low energies, the temperatures can be measured with a combined statistical and systematic uncertainty of just a few MeV, thus

showing that the experiment has a strong sensitivity to a possible flattening of the caloric curve. The acceptance corrected mass spectrum at $\sqrt{s_{NN}} = 8.8$ GeV, based on the assumption of no chiral mixing, is compared to the expectation in case of full chiral mixing in the right panel of Fig. 4. As shown, the statistical and systematic uncertainty provide a very good sensitivity to an increase of the yield due to chiral mixing of $\sim 20\text{--}30\%$.

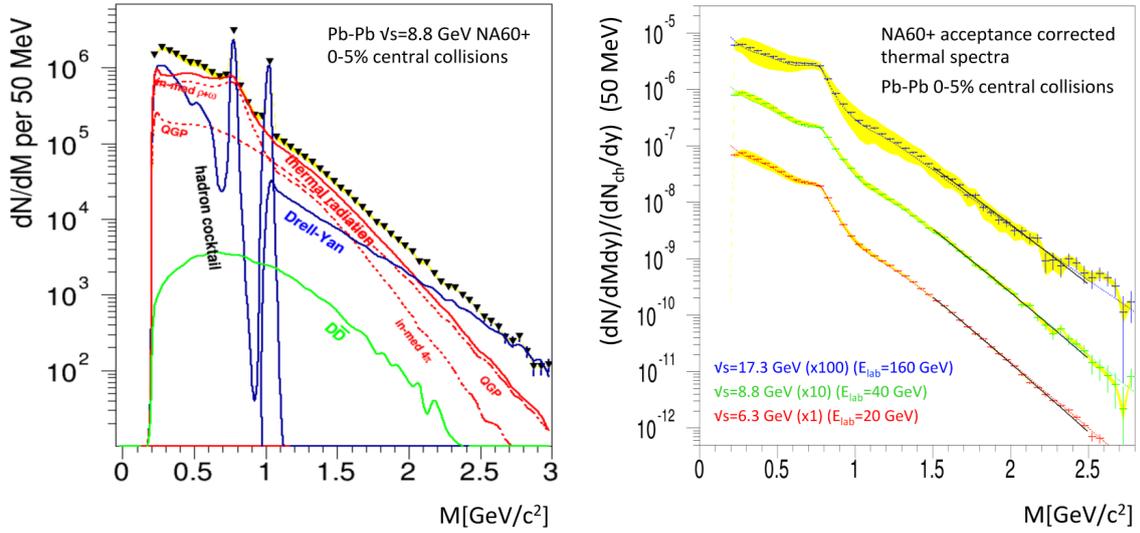


Fig. 3: (Left) expected signal sample in 5% most central Pb–Pb collision at $\sqrt{s_{NN}} = 8.8$ GeV after subtraction of combinatorial and fake match background. (Right) acceptance corrected thermal spectra at three different beam energies obtained after subtraction of open charm, Drell-Yan and hadronic cocktail below 1 GeV.

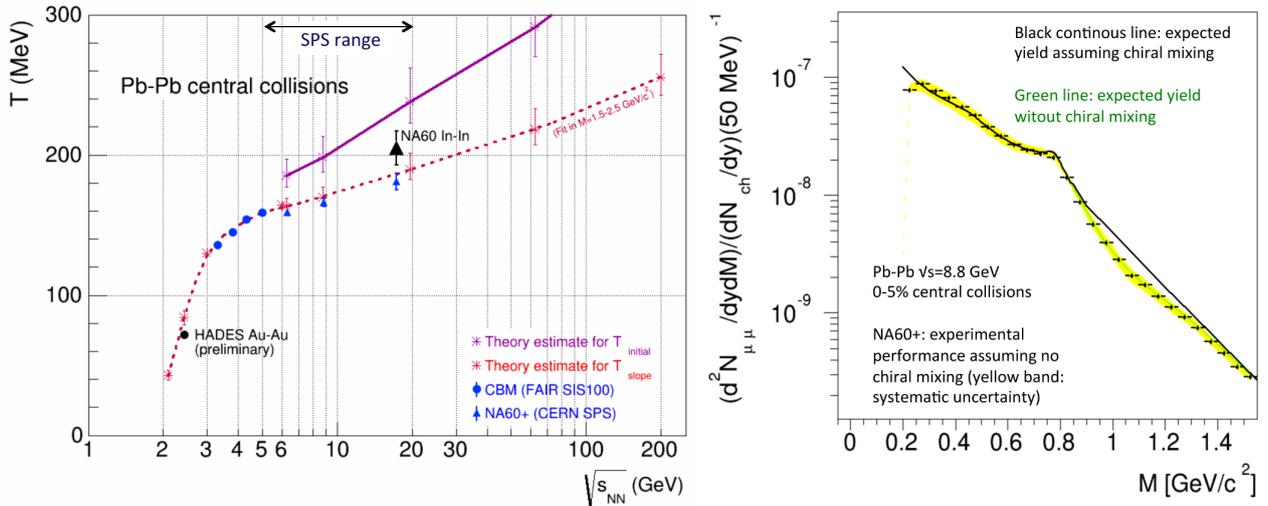


Fig. 4: (Left) medium temperature evolution vs $\sqrt{s_{NN}}$ in central Pb–Pb collisions. T_{initial} (magenta) and T_{slope} (red) are theoretical estimates for the initial medium temperature and the temperature from dilepton spectra respectively, using [12] and a coarse graining approach in UrQMD [41, 42]. Blue triangles are the expected performance from NA60+ (CBM performance is also shown). The only existing measurements at present are from NA60 In–In [5, 7] and from HADES Au–Au [43]. (Right) NA60+ projection for the acceptance corrected thermal dimuon mass spectrum at $\sqrt{s_{NN}} = 8.8$ GeV in case of no chiral mixing compared to the theoretical expectation (green line). The black line above 1 GeV is the expectation from full chiral mixing [12].

Finally the performance for the dilepton excitation function, i. e. the total thermal yield measurement in the mass range 0.3–0.7 GeV, is compared to the lifetime estimate of [12] in Fig. 5. The uncertainty is dominated by the systematic error from background subtraction. The measurement at low energies provides very good sensitivity to possible anomalies in the fireball lifetime.

5.2 Open charm measurements: hadronic decays of mesons/baryons

Open charm hadrons can be fully reconstructed with the NA60+ apparatus via their decays into two or three charged hadrons. In particular, the following decays could enable the measurement of non-strange and strange D mesons as well as Λ_c baryons: $D^0 \rightarrow K^- \pi^+$, $D^+ \rightarrow K^- \pi^+ \pi^+$, $D_s^+ \rightarrow \phi \pi^+ \rightarrow K^+ K^- \pi^+$, $\Lambda_c^+ \rightarrow p K^- \pi^+$ and their charge conjugates. The

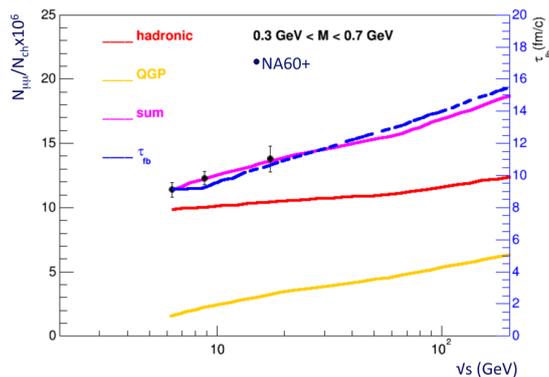


Fig. 5: Performance for thermal dilepton yield measurement for the fireball lifetime measurement.

decay particles (pions, kaons and protons) are detected by reconstructing their tracks in the silicon-pixel detectors of the VT. D-meson and Λ_c candidates are built combining pairs or triplets of tracks with the proper charge signs. The huge combinatorial background can be reduced via geometrical selections on the displaced decay-vertex topology, exploiting the fact that the mean proper decay lengths $c\tau$ of open charm hadrons are of about 60–310 μm , and therefore their decay vertices are typically displaced by a few hundred μm from the interaction vertex. Among the measurements proposed by NA60+, open-charm hadron studies are those that impose the strongest constraints on the design of the VT detectors, which should provide good resolution on the track parameters in order to allow us to separate the secondary tracks produced in open-charm hadron decays from the primary ones originating from the interaction point.

The benchmark studies were carried out for the measurement of $D^0 \rightarrow K^- \pi^+$ in the 5% most central Pb–Pb collisions at two different beam energies: 158 and 60 GeV/nucleon, corresponding to $\sqrt{s_{\text{NN}}} = 17.3$ and 10.6 GeV, respectively. The D^0 and \bar{D}^0 mesons were simulated with p_T and rapidity distributions obtained with the POWHEG-BOX event generator [44] for the hard-scattering and PYTHIA 6 for the parton shower and hadronization. The combinatorial background was estimated by simulating pions, kaons and protons with multiplicity, p_T and rapidity distributions taken from the parameterisations published by the NA49 collaboration in Refs. [45, 46]. The number of particles per event at $\sqrt{s_{\text{NN}}} = 17.3$ GeV is about 1200, which produce about 350k background candidates per event, out of which about 8000 have an invariant mass within 60 MeV from the D^0 -meson mass (1.865 GeV). The yield per event at $\sqrt{s_{\text{NN}}} = 17.3$ GeV, estimated assuming $\sigma_{c\bar{c}} = 5 \mu\text{b}$ (based on [47, 48] and POWHEG) and $f(c \rightarrow D^0) \sim 0.55$, is about 0.006. The signal-to-background ratio is therefore about $7 \cdot 10^{-7}$ and needs to be enhanced with the kinematical and geometrical selections.

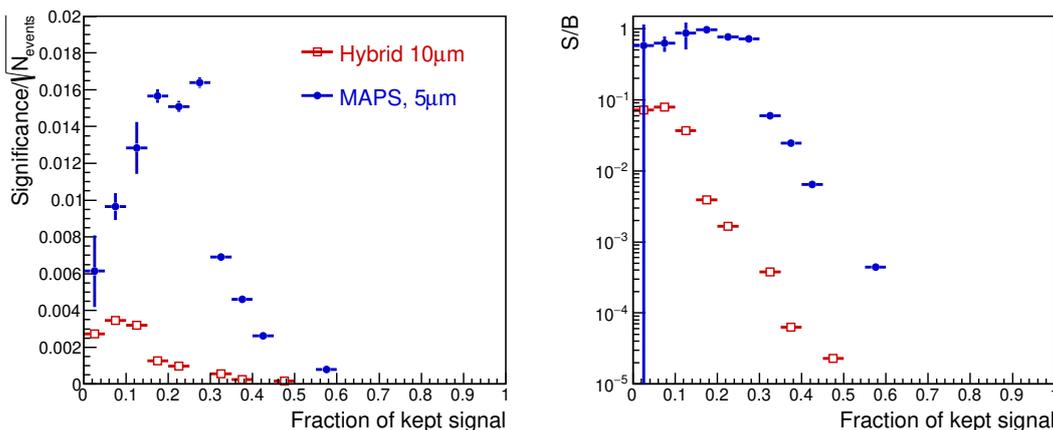


Fig. 6: D^0 -meson statistical significance (normalized to the square root of the number of events) and signal-over-background ratio as a function of the selection efficiency for the 5% most central Pb–Pb collisions at $\sqrt{s_{\text{NN}}} = 17.3$ GeV. The signal and the background yields are evaluated in a 2σ invariant-mass region around the D^0 peak.

Several selection sets were tested, and for each of them the signal-selection efficiency, the statistical significance of the signal ($S/\sqrt{S+B}$) and the signal-to-background ratio (S/B) were computed. In Fig. 6, the significance per event and the S/B at $\sqrt{s_{\text{NN}}} = 17.3$ GeV are shown as a function of the efficiency for two different configurations of the VT detectors, namely the one based on hybrid pixel sensors with 10 μm spatial resolution and the one based on Monolithic Active Pixels (MAPS) which feature a better spatial resolution (5 μm) and a reduced material budget. The performance is substantially better with the MAPS detector, which provides a better resolution on the decay track momentum, on the decay vertex position (10–15 μm in the plane transverse to the beam line with MAPS vs. 30–40 μm with hybrid pixels) and therefore

on the D^0 invariant mass (10 MeV vs. 24 MeV). In the left panel of Fig. 7, we show a projection for the invariant-mass distribution of D^0 candidates in $5 \cdot 10^9$ central Pb–Pb collisions at $\sqrt{s_{NN}} = 17.3$ GeV, corresponding to a sample of 10^{11} minimum bias (MB) collisions which can be collected in one month of data taking at 150 kHz of acquisition rate. The MAPS detector would enable a measurement of the D^0 -meson yield in central Pb–Pb collision with a statistical precision much better than 1%, which would allow also for studies in p_T and y intervals and for the determination of the elliptic flow coefficient v_2 of D mesons with percent level statistical uncertainty. In the right panel of Fig. 7, the projected performance for the 5% most central Pb–Pb collisions at $\sqrt{s_{NN}} = 10.6$ GeV is shown for the case of MAPS detectors. For this performance study we assumed $\sigma_{c\bar{c}} = 0.5 \mu\text{b}$ and the combinatorial background was simulated based on interpolation of NA49 measurements at 40 and 80 GeV/nucleon incident energy. It demonstrates that the integrated D^0 -meson cross section can be measured with statistical precision better than 1% at collision energies at which the charm cross section is poorly known experimentally.

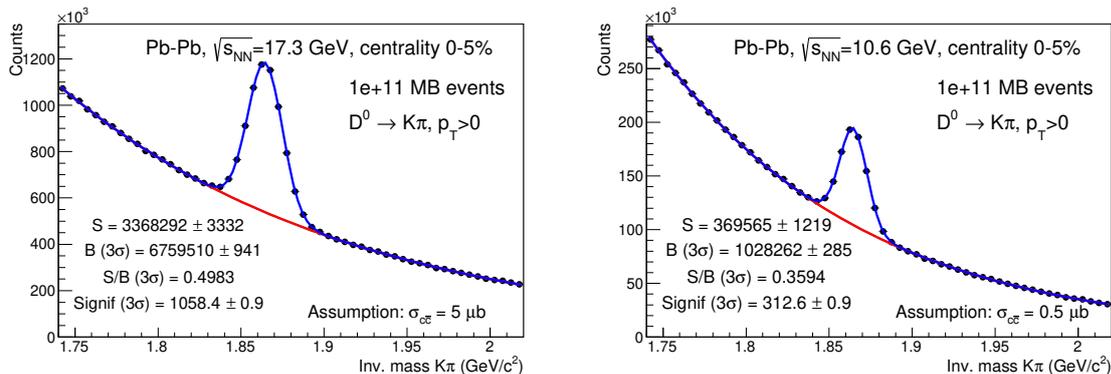


Fig. 7: Projection for invariant-mass distribution of D^0 candidates in $5 \cdot 10^9$ central Pb–Pb collisions at beam energies of 160 (left) and 60 (right) GeV/nucleon for the case of the VT detector based on MAPS with $5 \mu\text{m}$ spatial resolution.

The excellent performance obtained for the two-body decays of D^0 mesons suggests that open-charm measurements will also be feasible for three-body decay channels. This opens the possibility to measure the production yield of strange D mesons and of Λ_c baryons.

5.3 J/ψ suppression: onset of deconfinement

Among the measurements proposed by NA60+, quarkonium studies require the highest integrated luminosity L_{int} , due to the small production cross section at low incident beam energy. On the other hand, past SPS experiments (NA50/NA60) showed that the background levels in the dimuon invariant mass spectrum in the J/ψ region are also very small ($<5\%$) [49]. In addition, the NA60 experiment was able to perform a very accurate measurement of the centrality dependence of the suppression by collecting $\sim 3 \cdot 10^4$ J/ψ in In–In collisions at 158 GeV/nucleon incident energy, i. e. $\sqrt{s_{NN}} = 17.3$ GeV. In order to assess the possibility of a measurement with similar accuracy at lower incident energy, we have calculated the interaction rate needed in order to collect $3 \cdot 10^4$ J/ψ in a 30-day long Pb–Pb data taking period with NA60+. We have assumed (i) SPS burst structure similar to the one at top SPS energy, (ii) realistic values for the acceptance of the apparatus in the rapidity region $|y| < 0.5$ and (iii) a suppression of the J/ψ leading to a 2/3 reduction of the expected yields. Assuming a target thickness of 4 mm, we have also evaluated the corresponding beam intensity needed to collect the desired statistics. The result, shown in Fig. 8, shows that a large J/ψ sample can be collected while keeping the interaction rate below 1 MHz, corresponding to a beam intensity of about 10^7 Pb ions/s.

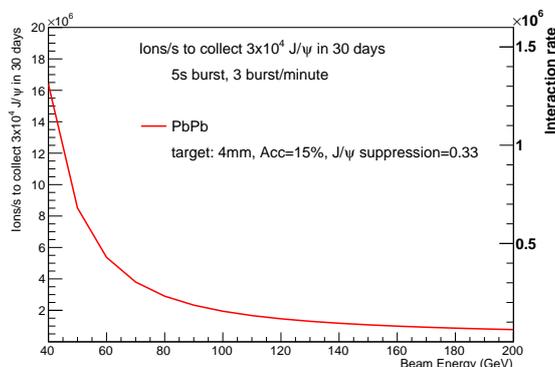


Fig. 8: Interaction rate and beam intensity needed to collect a sample of $3 \cdot 10^4$ J/ψ in Pb–Pb collisions at various energies.

At SPS energies, it is well known that the break-up of the J/ψ in cold nuclear matter plays an important role in determining the final observed yields in nucleus–nucleus collisions. Therefore, data taking with pA collisions are mandatory

to calibrate such an effect. We assumed to have 7 nuclear targets as mentioned in section 4 and 15 days of data taking at a beam intensity of $3 \cdot 10^8$ protons/s. In the left panel of Fig. 9, the expected cross sections as a function of the mass number A are shown, for an incident beam energy $E_{\text{lab}} = 50$ GeV, or $\sqrt{s_{\text{NN}}} = 9.8$ GeV, and in the hypothesis of a dissociation cross section $\sigma_{J/\psi-N} = 4.3$ mb. Such results are necessary in order to (i) evaluate the J/ψ production cross section $\sigma_{\text{pp} \rightarrow J/\psi X}$, needed for R_{AA} , (ii) extrapolate break-up effects to the geometrical conditions of Pb–Pb results. These procedures were well tested in past SPS experiments [50].

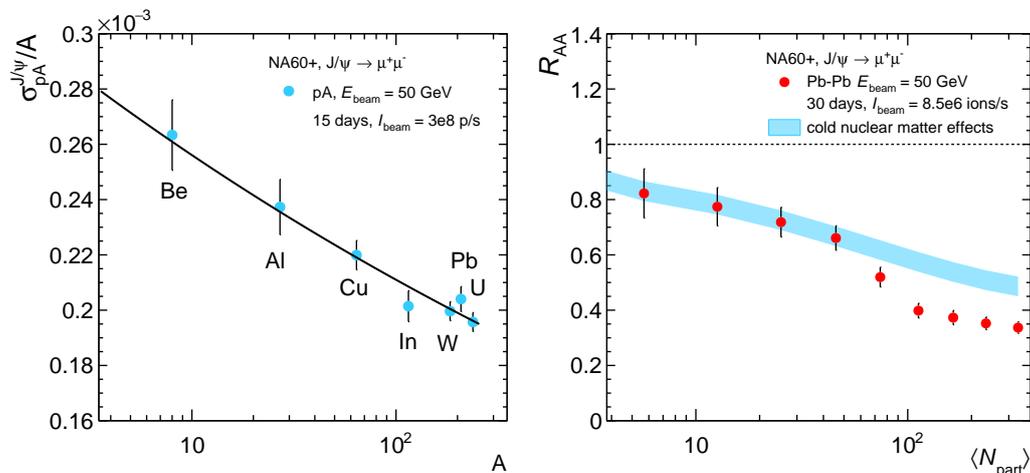


Fig. 9: (Left) J/ψ cross section normalized to the mass number A for pA collisions at $E_{\text{lab}} = 50$ GeV. The results of a fit using the parameterisation $\sigma_{\text{pA}}^{J/\psi} = \sigma_{\text{pp}}^{J/\psi} \cdot A^\alpha$ are shown. (Right) The nuclear modification factor for J/ψ production in Pb–Pb collisions at $E_{\text{lab}} = 50$ GeV as a function of N_{part} , compared with expectations from cold nuclear matter effects, obtained from the pA results and shown as a blue band.

Finally, the right panel of Fig. 9 shows the results of a simulation of the J/ψ R_{AA} as a function of the number of participant nucleons, N_{part} , assuming that for $N_{\text{part}} \lesssim 50$ the suppression is entirely due to cold nuclear matter effects, while for more central events an extra-suppression reaching 20% sets in. The simulation assumes 30 days of Pb–Pb collisions at $E_{\text{lab}} = 50$ GeV, with an SPS beam intensity of $8.5 \cdot 10^6$ Pb ions/s. The uncertainties shown for R_{AA} in the right panel of Fig. 9 include, in addition to the statistical uncertainty on the J/ψ , conservatively evaluated assuming a 20% background level, those on the evaluation of the centrality variables (Glauber model) and on the pp cross section, calculated from the pA results displayed in the left panel of Fig. 9. One can clearly see that a precise evaluation of a relatively small anomalous J/ψ suppression is within reach down to low E_{lab} .

Corresponding studies for the detection of the $\psi(2S) \rightarrow \mu^+ \mu^-$ and $\chi_c \rightarrow \mu^+ \mu^- \gamma$ decays are ongoing and are expected to nicely complement the physics programme of NA60+ in the charmonium sector.

6 Competition with present and future measurements

Several proposals have been put forward to investigate experimentally the QCD phase diagram at high μ_B in the next decade. Since thermal dilepton radiation, open charm and quarkonia are produced by rare processes, high precision measurements require very large interaction rates and operation in fixed target mode. Moreover, the μ_B interval accessible by a single experiment should be as wide as possible. The combination of these two key aspects is such that the physics programme described in this document can be uniquely pursued at the CERN SPS. Although other facilities for the study of ultra-relativistic heavy-ion collisions in the high- μ_B domain are being built (FAIR, NICA) they are either lacking the necessary interaction rate (NICA) or reach too low energy (SIS100 at FAIR) to address all the physics topics addressed by NA60+. Similarly, the beam energy scan programme at RHIC (BES-II) covers the same energy range as the CERN SPS, but with interaction rates lower by orders of magnitude. It should be noted that NA60+ and CBM with their high-interaction rates but different collision energies would nicely complement each other in mapping out, e. g. the caloric curve.

7 Conclusions

The exploration of the high- μ_B region of the QCD phase diagram represents one of the main directions in the evolution of the field of ultrarelativistic heavy-ion collisions. This document, submitted to the European Strategy for Particle Physics, summarizes the status of the NA60+ project, which aims at performing a comprehensive measurement, in the energy range accessible to the CERN SPS, of hard and electromagnetic processes, with unprecedented accuracy. The addressed observables include the production of thermal muon pairs from the QGP phase, the investigation of the modifications of the vector meson spectral functions as well as the study of charmonia and open charm mesons/baryons. Preliminary physics performance studies discussed in this document show that a set-up which makes use of existing advanced detection techniques would be able to carry out the proposed physics programme, provided that the experiment can profit of high-intensity ion beams as those that can be delivered in the ECN3 experimental hall.

Acknowledgements

We would like to thank F. Bergsma and P. A. G. Giudici (both CERN) for their contribution on the study of the toroidal magnet.

References

- [1] S. Borsanyi *et al.*, “Full result for the QCD equation of state with $2 + 1$ flavors,” *Phys. Lett.* **B730** (2014) 99, arXiv:1309.5258 [hep-lat].
- [2] C. Ratti, “Lattice QCD and heavy ion collisions: a review of recent progress,” *Rept. Prog. Phys.* **81** (2018) 084301, arXiv:1804.07810 [hep-lat].
- [3] **Wuppertal-Budapest** Collaboration, S. Borsanyi *et al.*, “Is there still any T_c mystery in lattice QCD? Results with physical masses in the continuum limit III,” *JHEP* **09** (2010) 073, arXiv:1005.3508 [hep-lat].
- [4] **NA60** Collaboration, A. Baldit *et al.*, “Study of prompt dimuon and charm production with proton and heavy ion beams at the CERN SPS: Proposal,” <http://cds.cern.ch/record/430343>.
- [5] **NA60** Collaboration, R. Arnaldi *et al.*, “Evidence for the production of thermal-like muon pairs with masses above $1 \text{ GeV}/c^2$ in 158 AGeV Indium–Indium Collisions,” *Eur. Phys. J.* **C59** (2009) 607, arXiv:0810.3204 [nucl-ex].
- [6] **NA60** Collaboration, R. Arnaldi *et al.*, “First measurement of the rho spectral function in high-energy nuclear collisions,” *Phys. Rev. Lett.* **96** (2006) 162302, arXiv:nucl-ex/0605007 [nucl-ex].
- [7] **NA60** Collaboration, H. J. Specht, “Thermal Dileptons from Hot and Dense Strongly Interacting Matter,” *AIP Conf. Proc.* **1322** (2010) 1, arXiv:1011.0615 [nucl-ex].
- [8] R. Rapp and J. Wambach, “Low mass dileptons at the CERN SPS: Evidence for chiral restoration?,” *Eur. Phys. J.* **A6** (1999) 415, arXiv:hep-ph/9907502 [hep-ph].
- [9] H. van Hees and R. Rapp, “Dilepton Radiation at the CERN Super Proton Synchrotron,” *Nucl. Phys.* **A806** (2008) 339, arXiv:0711.3444 [hep-ph].
- [10] **Particle Data Group**, M. Tanabashi, *et al.*, “Review of Particle Physics,” *Phys. Rev.* **D98** (2018) 030001.
- [11] M. Dey *et al.*, “Mixing of vector and axial mesons at finite temperature: an indication towards chiral symmetry restoration,” *Phys. Lett.* **B252** (1990) 620.
- [12] R. Rapp and H. van Hees, “Thermal dileptons as fireball thermometer and chronometer,” *Phys. Lett.* **B753** (2016) 586.
- [13] J. Pochodzalla *et al.*, “Probing the nuclear liquid–gas phase transition,” *Phys. Rev. Lett.* **75** (1995) 1040.
- [14] T. Matsui and H. Satz, “ J/ψ Suppression by Quark-Gluon Plasma Formation,” *Phys. Lett.* **B178** (1986) 416.
- [15] **NA50** Collaboration, B. Alessandro *et al.*, “A new measurement of J/ψ suppression in Pb–Pb collisions at 158 GeV per nucleon,” *Eur. Phys. J.* **C39** (2005) 335, arXiv:hep-ex/0412036 [hep-ex].
- [16] **PHENIX** Collaboration, A. Adare *et al.*, “ J/ψ suppression at forward rapidity in Au+Au collisions at $\sqrt{s_{NN}} = 200 \text{ GeV}$,” *Phys. Rev.* **C84** (2011) 054912, arXiv:1103.6269 [nucl-ex].
- [17] **ALICE** Collaboration, J. Adam *et al.*, “ J/ψ suppression at forward rapidity in Pb–Pb collisions at $\sqrt{s_{NN}} = 5.02 \text{ TeV}$,” *Phys. Lett.* **B766** (2017) 212, arXiv:1606.08197 [nucl-ex].
- [18] **NA60** Collaboration, R. Arnaldi *et al.*, “ J/ψ production in proton–nucleus collisions at 158 and 400 GeV,” *Phys. Lett.* **B706** (2012) 263, arXiv:1004.5523 [nucl-ex].
- [19] A. Beraudo *et al.*, “Extraction of Heavy-Flavor Transport Coefficients in QCD Matter,” *Nucl. Phys.* **A979** (2018) 21, arXiv:1803.03824 [nucl-th].
- [20] S. Plumari, V. Minissale, S. K. Das, G. Coci, and V. Greco, “Charmed Hadrons from Coalescence plus Fragmentation in relativistic nucleus–nucleus collisions at RHIC and LHC,” *Eur. Phys. J.* **C78** (2018) 348, arXiv:1712.00730 [hep-ph].
- [21] M. He, R. J. Fries, and R. Rapp, “Thermal Relaxation of Charm in Hadronic Matter,” *Phys. Lett.* **B701** (2011) 445, arXiv:1103.6279 [nucl-th].

- [22] F. Scardina, S. K. Das, V. Minissale, S. Plumari, and V. Greco, “Estimating the charm quark diffusion coefficient and thermalization time from D meson spectra at energies available at the BNL Relativistic Heavy Ion Collider and the CERN Large Hadron Collider,” *Phys. Rev.* **C96** (2017) 044905, arXiv:1707.05452 [nucl-th].
- [23] NA49 Collaboration, C. Alt *et al.*, “Upper limit of D^0 production in central Pb–Pb collisions at 158 AGeV,” *Phys. Rev.* **C73** (2006) 034910, arXiv:nucl-ex/0507031 [nucl-ex].
- [24] B. Friman, C. Hohne, J. Knoll, S. Leupold, J. Randrup, R. Rapp, and P. Senger, “The CBM physics book: Compressed baryonic matter in laboratory experiments,” *Lect. Notes Phys.* **814** (2011) 1.
- [25] K. J. Eskola, P. Paakkinen, H. Paukkunen, and C. A. Salgado, “EPPS16: Nuclear parton distributions with LHC data,” *Eur. Phys. J.* **C77** (2017) 163, arXiv:1612.05741 [hep-ph].
- [26] G. Aglieri Rinella *et al.*, “The ALPIDE pixel sensor chip for the upgrade of the ALICE Inner Tracking System,” *Nucl. Instrum. Meth.* **A845** (2017) 583. Proceedings of the Vienna Conference on Instrumentation 2016.
- [27] ALICE Collaboration, “Expression of Interest for an ALICE ITS Upgrade in LS3,” <https://cds.cern.ch/record/2644611/files/ITS3%20EoI.5.pdf>.
- [28] F. Sauli, “GEM: A new concept for electron amplification in gas detectors,” *Nucl. Instrum. Meth.* **A386** (1997) 531.
- [29] Altunbas, C. and others, “Construction, test and commissioning of the triple-GEM tracking detectors for COMPASS,” *Nucl. Instrum. Meth.* **A490** (2002) 177.
- [30] G. Bencivenni *et al.*, “A triple GEM detector with pad readout for high rate charged particle triggering,” *Nucl. Instrum. Meth.* **A488** (2002) 493.
- [31] M. Bagliesi *et al.*, “The TOTEM T2 telescope based on triple-GEM chambers,” *Nucl. Instrum. Meth.* **A617** (2010) 134.
- [32] D. Abbaneo *et al.*, “Upgrade of the CMS muon system with triple-GEM detectors,” *JINST* **9** (2014) C10036.
- [33] ALICE Collaboration, “Upgrade of the ALICE Time Projection Chamber,” Tech. Rep. CERN-LHCC-2013-020. ALICE-TDR-016, CERN, Geneva, 2013. <https://cds.cern.ch/record/1622286>.
- [34] M. Villa *et al.*, “Progress on large area GEMs,” *Nucl. Instrum. Meth.* **A628** (2011) 182. VCI 2010.
- [35] A. Zhang *et al.*, “A GEM readout with radial zigzag strips and linear charge-sharing response,” *Nucl. Instrum. Meth.* **A887** (2018) 184.
- [36] P. Aspell, G. Anelli, P. Chalmet, J. Kaplon, K. Kloukinas, H. Mugnier, and W. Snoeys, “VFAT2: A front-end system on chip providing fast trigger information, digitized data storage and formatting for the charge sensitive readout of multi-channel silicon and gas particle detectors,” <http://cds.cern.ch/record/1069906>.
- [37] ATLAS Collaboration, G. Iakovidis, “VMM3, an ASIC for Micropattern Detectors,” Tech. Rep. ATL-MUON-PROC-2018-003, CERN, Geneva, 2018. <http://cds.cern.ch/record/2309951>.
- [38] L. Anderson *et al.*, “A high resolution spectrometer for the study of high mass muon pairs produced by intense hadron beams,” *Nuclear Instruments and Methods in Physics Research* **223** (1984) 26.
- [39] F. Bergsma and P. Giudici, “A general-purpose toroidal spectrometer magnet—conceptual study for the NA60+ proposal,”.
- [40] F. Becattini, J. Manninen, and M. Gazdzicki, “Energy and system size dependence of chemical freeze-out in relativistic nuclear collisions,” *Phys. Rev.* **C73** (2006) 044905, arXiv:hep-ph/0511092 [hep-ph].
- [41] S. Endres, H. van Hees, J. Weil, and M. Bleicher, “Dilepton production and reaction dynamics in heavy-ion collisions at SIS energies from coarse-grained transport simulations,” *Phys. Rev.* **C92** (2015) 014911.
- [42] T. Galatyuk, “Future facilities for high μ_b physics,” *to be published in Quark Matter 2018 conference proceedings* .
- [43] HADES Collaboration, S. Harabasz *et al.*, “Multi-differential pattern of low-mass e^+e^- excess from $\sqrt{s_{NN}} = 2.4$ GeV Au–Au collisions with HADES,” *to be published in Quark Matter 2018 conference proceedings* .
- [44] S. Alioli, P. Nason, C. Oleari, and E. Re, “A general framework for implementing NLO calculations in shower Monte Carlo programs: the POWHEG BOX,” *JHEP* **06** (2010) 043, arXiv:1002.2581 [hep-ph].
- [45] NA49 Collaboration, S. V. Afanasiev *et al.*, “Energy dependence of pion and kaon production in central Pb+Pb collisions,” *Phys. Rev.* **C66** (2002) 054902, arXiv:nucl-ex/0205002 [nucl-ex].

- [46] **NA49** Collaboration, C. Alt *et al.*, “Energy and centrality dependence of anti-p and p production and the anti-Lambda/anti-p ratio in Pb+Pb collisions between 20 AGeV and 158 AGeV,” *Phys. Rev.* **C73** (2006) 044910.
- [47] C. Lourenco and H. K. Wohri, “Heavy flavour hadro-production from fixed-target to collider energies,” *Phys. Rept.* **433** (2006) 127, arXiv:hep-ph/0609101 [hep-ph].
- [48] **Hard Probe** Collaboration, R. Vogt, “The A dependence of open charm and bottom production,” *Int. J. Mod. Phys.* **E12** (2003) 211, arXiv:hep-ph/0111271 [hep-ph].
- [49] **NA60** Collaboration, R. Arnaldi *et al.*, “ J/ψ production in indium-indium collisions at 158 GeV/nucleon,” *Phys. Rev. Lett.* **99** (2007) 132302.
- [50] **NA50** Collaboration, B. Alessandro *et al.*, “Charmonia and Drell-Yan production in proton–nucleus collisions at the CERN SPS,” *Phys. Lett.* **B553** (2003) 167.

Appendix: NA60+ Collaboration

M. Agnello^{14,16}, F. Antinori¹², H. Appelshäuser², R. Arnaldi¹⁴, R. Bailhache², L. Barioglio^{17,14}, S. Beole^{17,14}, A. Beraudo¹⁴, A. Bianchi^{17,14}, L. Bianchi^{17,14}, E. Botta^{17,14}, E. Bruna¹⁴, S. Bufalino^{16,14}, E. Casula^{7,8}, F. Catalano^{16,14}, S. Chattopadhyay⁶, A. Chauvin⁷, C. Cicalo⁷, M. Concas^{15,14}, P. Cortese^{18,14}, T. Dahms^{4,5,i}, A. Dainese¹², A. Das⁶, D. Das⁶, D. Das⁶, I. Das⁶, L. Das Bose⁶, A. De Falco⁷, N. De Marco¹⁴, S. Delsanto^{17,14}, A. Drees²², L. Fabbietti⁵, P. Fecchio^{16,14}, A. Ferretti^{17,14}, A. Feliciello¹⁴, M. Gagliardi^{17,14}, P. Gasik⁵, F. Geurts²¹, P. Giubilato^{12,13}, V. Greco⁹, F. Grosa^{16,14}, H. Hansen¹, J. Klein¹⁴, W. Li²¹, M.P. Lombardo¹¹, M. Maserà^{17,14}, A. Masoni⁷, L. Micheletti^{17,14}, L. Musa²⁰, M. Nardi¹⁴, H. Onishi¹⁹, C. Oppedisano¹⁴, B. Paul^{7,8}, S. Plumari¹⁰, F. Prino¹⁴, M. Puccio^{17,14}, L. Ramello^{18,14}, R. Rapp²³, I. Ravasenga^{16,14}, A. Rossi^{12,13}, P. Roy⁶, E. Scomparin^{14,i}, S. Siddhanta⁷, R. Shahoyan²⁰, T. Sinha⁶, M. Sitta^{18,14}, H. Specht³, S. Trogolo^{17,14}, R. Turrisi¹², A. Uras¹, G. Usai^{7,8,i,ii}, E. Vercellin^{17,14}, J. Wiechula²

Notes

ⁱ Editors

ⁱⁱ E-mail: gianluca.usai@ca.infn.it

Collaboration Institutes

- ¹ Université de Lyon, Université Lyon 1, CNRS/IN2P3, IPN-Lyon, Villeurbanne, Lyon, France
- ² Institut für Kernphysik, Johann Wolfgang Goethe-Universität Frankfurt, Frankfurt, Germany
- ³ Physikalisches Institut, Ruprecht-Karls-Universität Heidelberg, Heidelberg, Germany
- ⁴ Excellence Cluster ‘Universe’, Technische Universität München, Munich, Germany
- ⁵ Physik Department, Technische Universität München, Munich, Germany
- ⁶ Saha Institute of Nuclear Physics, Homi Bhabha National Institute, Kolkata, India
- ⁷ INFN, Sezione di Cagliari, Cagliari, Italy
- ⁸ Dipartimento di Fisica dell’Università di Cagliari, Cagliari, Italy
- ⁹ INFN, Laboratori Nazionali del Sud, Catania, Italy
- ¹⁰ Dipartimento di Fisica e Astronomia dell’Università di Catania, Catania, Italy
- ¹¹ INFN, Laboratori Nazionali di Frascati, Frascati, Italy
- ¹² INFN, Sezione di Padova, Padova, Italy
- ¹³ Dipartimento di Fisica e Astronomia dell’Università di Padova, Padova, Italy
- ¹⁴ INFN, Sezione di Torino, Turin, Italy
- ¹⁵ Dipartimento DET del Politecnico di Torino, Turin, Italy
- ¹⁶ Dipartimento DISAT del Politecnico di Torino, Turin, Italy
- ¹⁷ Dipartimento di Fisica dell’Università di Torino, Turin, Italy
- ¹⁸ Dipartimento di Scienze e Innovazione Tecnologica dell’Università del Piemonte Orientale, Alessandria, Italy
- ¹⁹ Research Center for Electron Photon Science (ELPH), Tohoku University, Sendai, Japan
- ²⁰ European Organization for Nuclear Research (CERN), Geneva, Switzerland
- ²¹ Department of Physics and Astronomy, Rice University, Houston, Texas, USA
- ²² Department of Physics and Astronomy, Stony Brook University, SUNY, Stony Brook, New York, USA
- ²³ Cyclotron Institute and Department of Physics and Astronomy, Texas A&M University, College Station, Texas, USA